**CSIRO** PUBLISHING

*Aust. J. Chem.*
http://dx.doi.org/10.1071/CH14722

**Full Paper**

# Synthesis, Characterization, and Nanocatalysis Application of Core–Shell Superparamagnetic Nanoparticles of $Fe_3O_4$@Pd

*Ariel L. Cappelletti,*[A] *Paula M. Uberman,*[B] *Sandra E. Martín,*[B] *Martín E. Saleta,*[C] *Horacio E. Troiani,*[C] *Rodolfo D. Sánchez,*[C] *Raúl E. Carbonio,*[D] *and Miriam C. Strumia*[A,E]

[A]IMBIV-CONICET, Departamento de Química Orgánica, Facultad de Ciencias Químicas, Universidad Nacional de Córdoba, X5000HUA Córdoba, Argentina.
[B]INFIQC-CONICET, Departamento de Química Orgánica, Facultad de Ciencias Químicas, Universidad Nacional de Córdoba, X5000HUA Córdoba, Argentina.
[C]Centro Atómico Bariloche, Comisión Nacional de Energía Atómica and Instituto Balseiro, Universidad Nacional de Cuyo, 8400 San Carlos de Bariloche (RN), Argentina.
[D]INFIQC-CONICET, Departamento de Fisicoquímica, Facultad de Ciencias Químicas, Universidad Nacional de Córdoba, X5000HUA Córdoba, Argentina.
[E]Corresponding author. Email: mcs@fcq.unc.edu.ar

There is a wide number of different synthetic methods to obtain magnetite ($Fe_3O_4$) superparamagnetic nanoparticles (SPNPs). However, only a few are able to produce very small and well defined SPNPs with narrow size distribution. We report a modification of the metal-complex decomposition in organic media method in which we replace iron(III) acetylacetonate ($Fe(Acac)_3$) with an iron–urea complex (Fe-Urea) as metal source for the synthesis. With this modification we were able to obtain small particle sizes with a good control in size distribution. The Fe-Urea complex is easy to prepare with excellent yields. Core–shell nanoparticles are then prepared using palladium(II) acetylacetonate as a Pd source, to obtain a $Pd^0$ shell stabilised by oleylamine. The core–shell superparamagnetic nanoparticles of $Fe_3O_4$@Pd-OA are extensively characterized by FT-IR, powder X-ray diffraction, transmission electron microscopy, UV-vis, thermogravimetric analysis/differential scanning calorimetry, and magnetic susceptibility measurements, and tested in a palladium-catalyzed cross-coupling Suzuki–Miyaura reaction with promising results.

Manuscript received: 19 December 2014.
Manuscript accepted: 14 March 2015.
Published online: 21 May 2015.

## Introduction

In recent years, the amount of scientific research on magnetic nanoparticles (MNPs) has increased significantly. This is due to their versatility for use in so many different applications, ranging from industrial (magnetic fluid seal, magnetic fluidic sensors, etc.)[1] to biomedical fields (magnetic resonance imaging (MRI),[2] hyperthermia,[3] drug delivery, etc.).[4,5] Of particular interest is their magnetization, which makes them suitable for use in a wide range of applications.[6–8] It is known that the magnetization is strongly related to the magnetic particle's size and shape. For example, the ferromagnetic iron oxides such as maghemite and magnetite lose their remanent magnetization if they are <30 nm in diameter, however superparamagnetic nanoparticles (SPNPs) can be obtained bellow this diameter.[9]

Magnetite ($Fe_3O_4$) NPs have become extensively studied magnetic materials. The main reasons for this are principally their active surface chemical functionality, biocompatibility, and low cost. Their chemical stability is generally referred to as another advantage, however, under an aerobic atmosphere magnetite is often oxidized to maghemite ($\gamma$-$Fe_2O_3$).[10]

The common employed synthesis methods for obtaining magnetite particles are co-precipitation,[11,12] sol–gel processes, process-based microemulsions,[13] etc., however all these methods despite their efficiency have different types of disadvantages. Moreover, the obtained particles using these methods usually present quite wide size distributions and low crystallinity, affecting their magnetic properties. Therefore, numerous research groups are dedicated to the study of the optimization of their synthesis, conserving the distinctive properties of the MNPs.

An important field of application for NPs is nanocatalysis, as a result of the extremely small size, high surface-to-volume ratio, and novel properties of NPs. In the last decade the development of high-performance palladium nanoparticle (PdNP) catalysts has been an important area of research, and consequently, the synthetic methods with a rigorous control of the NPs size has become a leading research focus.[14–16]

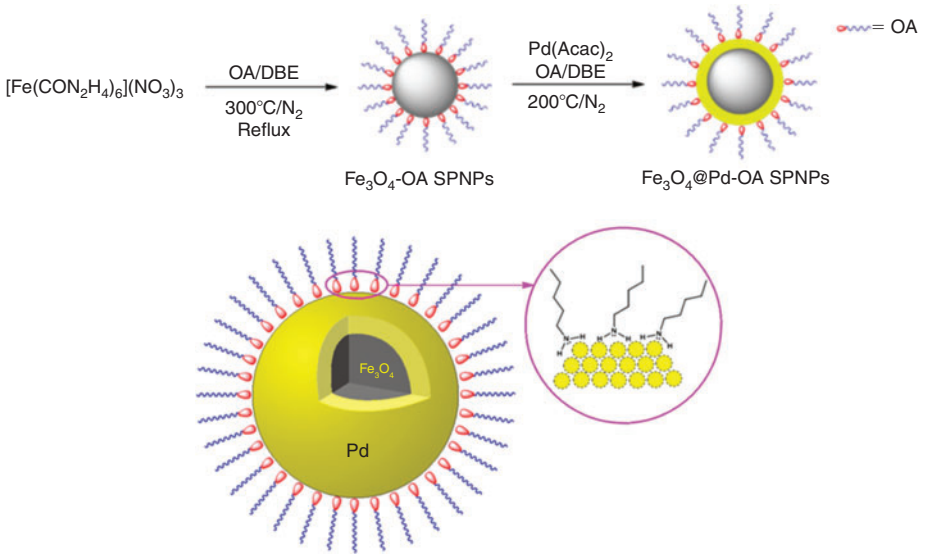


**Fig. 1.** Synthesis of precursors, $Fe_3O_4$-OA and $Fe_3O_4$@Pd-OA superparamagnetic nanoparticles (SPNPs) (OA, oleylamine; DBE, dibenzylether).

Palladium represents one of the most used catalysts in advanced organic syntheses, which is mainly applied in the formation of C–C bonds. Among the main coupling reactions, a special place is occupied by the Suzuki–Miyaura reaction,[17–21] a very attractive reaction from a catalytic perspective and one of the most powerful tools in C–C bond formation. Many homogeneous catalysts have been developed for the Suzuki–Miyaura coupling based on palladium complexes in the presence of different ligands.[22–28] Despite the remarkable progress achieved in this area, the typical problems associated with all homogeneous catalysts, that is, the separation of the catalyst from the reaction products and the catalyst recovery, are the major limitations of these catalytic systems. Alternatively, heterogeneous palladium catalysts have been developed in order to improve catalyst stability and handling during workup procedures and recycling.[18] However, the active sites in heterogeneous catalysts are less accessible than in a homogeneous system, and thus the overall activity of the catalyst system is decreased. Accordingly, the nanocatalysis that combines high activity, stability, and recyclability offers an attractive alternative to conventional catalysis.[14–16] However, the isolation and recovery of nanocatalysts from the reaction mixture is not easy. To overcome this problem, the use of MNPs has emerged as a useful solution, since the separation of nanocatalysts can be achieved using an external magnet.[29] Although MNPs have been developed for biological and medical applications, recently an important number of articles dedicated to the applications of MNPs in catalysis have been published, particularly in the Suzuki–Miyaura coupling reaction.[29–36]

Herein we report a novel and easy synthesis methodology of core–shell SPNPs with a $Fe_3O_4$ core and a very thin Pd shell. A detailed characterization of $Fe_3O_4$ and $Fe_3O_4$@Pd NPs is presented using different techniques. This new synthetic method proved to be an efficient way to protect $Fe_3O_4$ from oxidation and to provide an efficient and reusable catalyst for the Suzuki–Miyaura coupling reaction.

## Results and Discussion

Core–shell SPNPs consisting of a core of magnetite and a shell of oleylamine (OA)-stabilized Pd ($Fe_3O_4$@Pd-OA) were prepared by a chemical method involving the decomposition of organic metal complexes in organic media.

First, $Fe_3O_4$ SPNPs were synthesized by the decomposition of a Fe-Urea complex ($[Fe(CON_2H_4)_6](NO_3)_3$) in a mixture of OA and DBE (dibenzyl ether) at 300°C. Second, using the SPNPs of $Fe_3O_4$ as seeds, the Pd shell was achieved through the decomposition of $Pd(Acac)_2$ in the same solvent mixture at 200°C.

The Fe-Urea complex was used in order to study if the Fe precursors normally used ($Fe(Acac)_3$ or $Fe(CO)_5$) can be replaced, and the effects on the product's properties produced by this replacement. The core–shell SPNPs obtained were extensively characterized, involving a novel method to distinguish $Fe_3O_4$ from $\gamma$-$Fe_2O_3$ by FT-IR spectroscopy. $Fe_3O_4$@Pd-OA SPNPs presented high purity, good crystallinity, and acceptable polydispersity. In addition, the SPNPs of $Fe_3O_4$@Pd-OA showed good catalytic activity in Suzuki cross-coupling reactions.

The schematic procedure for the synthesis of the SPNPs can be seen on Fig. 1.

There are several reports of the synthesis, characterization, and thermal behaviour of the Fe-Urea complex,[37–40] but unfortunately, they are difficult to reproduce and in some cases, lead to an orange powder. For this reason, the development of an easy method to obtain a highly pure light-green powder consisting of a Fe-Urea complex was optimized. In a further step, this product was the precursor for the synthesis of core–shell SPNPs with catalytic properties.

To perform the synthesis of the Fe-Urea complex, the reaction of $Fe(NO_3)_3 \cdot 9H_2O$ with urea in ethanol was carried out. The addition of $HNO_3$ is essential to avoid the formation of $Fe(OH)_3$ (orange), which precipitates at pH values of 3 or greater. By controlling the pH of the reaction mixture, a light-green powder consisting of a pure Fe-Urea complex is obtained.

Next, the pure Fe-Urea complex was used to synthesize the $Fe_3O_4$-OA SPNPs by thermal decomposition in organic media. It is important to note that the thermal decomposition of the Fe-Urea complex can lead to the formation of toxic compounds, e.g. HCNO, as determined by Carp et al.[40] For this reason, the reaction was carried out first at 155°C for 1 h, and then at 300°C for 1 h to diminish the formation of these toxic compounds.

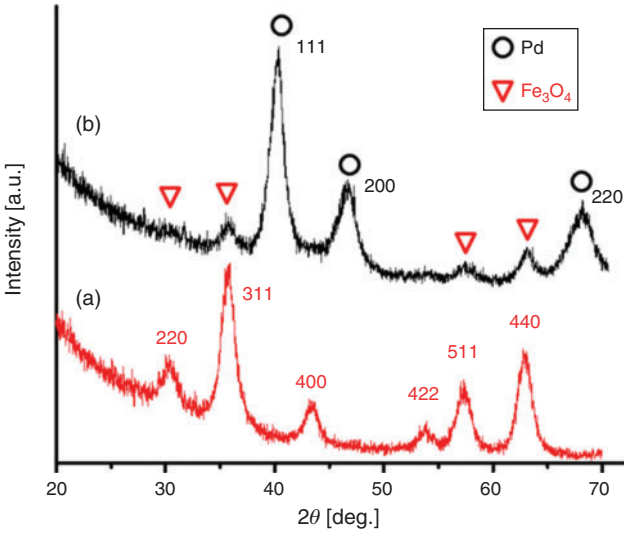


**Fig. 2.** Powder X-ray diffraction pattern of (a) $Fe_3O_4$-OA and (b) $Fe_3O_4$@Pd-OA superparamagnetic nanoparticles, with the Miller indexes in both cases (OA, oleylamine).

Finally, in order to diminish the crystal growth of the $Fe_3O_4$-OA seeds and considering that the flash point of $Pd(Acac)_2$ is near to 205°C, the palladium shell was achieved by the decomposition of $Pd(Acac)_2$ at 200°C.

### *Characterization of $Fe_3O_4$-OA and $Fe_3O_4$@Pd-OA SPNPs*

The first step in the synthetic pathway leads to highly pure small $Fe_3O_4$-OA SPNPs which exhibit typical powder X-ray diffraction (PXRD) peaks of the $Fe_3O_4$ phase at around 30.49, 35.81, 43.48, 53.90, 57.27, and 62.95 degrees ($2\theta$), which correspond to the (220), (311), (400), (422), (511), and (440) reflections, respectively (Fig. 2a). The second stage of the synthesis leads to $Fe_3O_4$@Pd-OA SPNPs, where the peaks of fcc Pd at around 39.82, 46.09, and 67.25 ($2\theta$), which correspond to the (111), (200), and (220) reflections are present, respectively (Fig. 2b), in addition to the reflections due to the $Fe_3O_4$ phase.

Rietveld refinements of the magnetite and core–shell SPNPs were performed (Figs S1 and S2, Supplementary Material). The structure of both SPNPs can be well described with the cubic space groups *Fd-3m* and *Fm-3m* for the $Fe_3O_4$ and Pd phases respectively. Tables in Figs S1 and S2 summarize the refined structural data for the $Fe_3O_4$-OA and $Fe_3O_4$@Pd-OA SPNPs.

In Fig. S3 (Supplementary Material) a selected area electron diffraction (SAED) pattern of the SPNPs $Fe_3O_4$ is presented. The pattern confirms the high crystallinity of the magnetite sample and that the crystallites are randomly oriented. To index the pattern the intensity profiles from several directions in the reciprocal space was measured and from the distances of the reciprocal space the interplanar *d*-distance was calculated. Intensity profiles from several directions as a function of *d*-distance are plotted in Fig. S3b. The peaks were indexed in good agreement with the (*hkl*) indices of the cubic spinel structure of magnetite. From the *d*-distance and the indices a cubic cell parameter $a = 8.26$ Å was obtained; this value is close to the cell parameter reported in the bibliography and to the one obtained in the present paper by PXRD.

The FT-IR spectra of $Fe_3O_4$-OA SPNPs (Fig. S4, Supplementary Material) is highly consistent with that previously reported, showing the typical low frequency bands of the spinel $Fe_3O_4$ at 586 $cm^{-1}$, which is related to Fe–O deformation in

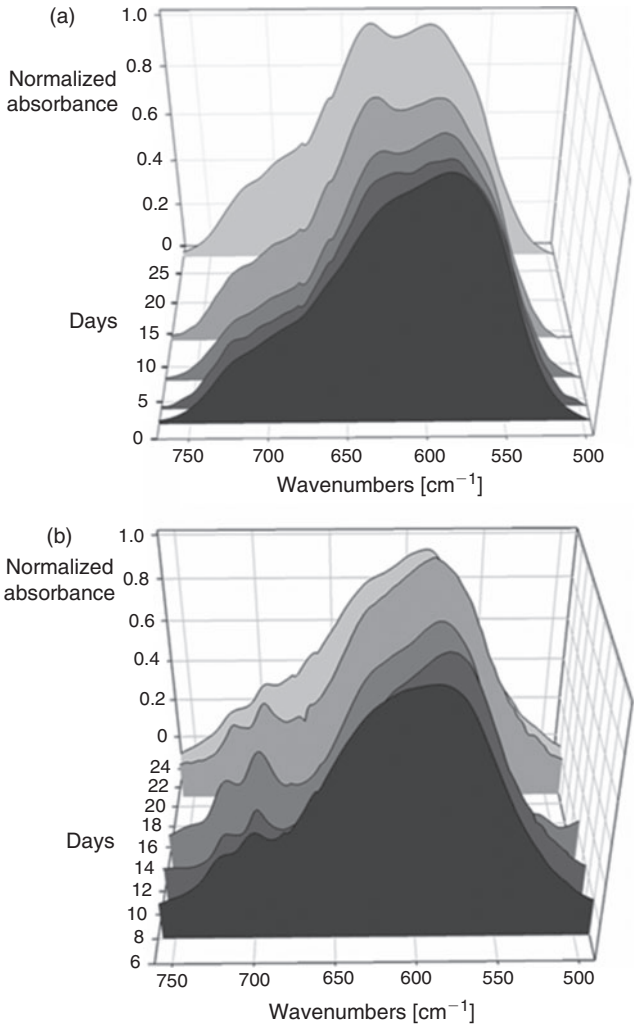


**Fig. 3.** FT-IR spectra of superparamagnetic nanoparticles of (a) $Fe_3O_4$-OA and (b) $Fe_3O_4$@Pd-OA as a function of time (OA, oleylamine).

octahedral and tetrahedral sites, and the band at 417 $cm^{-1}$, referred to as Fe–O deformation in octahedral sites, while the bands at 1330–1650 $cm^{-1}$ are due to the $-NH_2$ bending mode, and the bands around 2920 and 2850 $cm^{-1}$ are for methyl stretching.[41,42] The FT-IR spectrum of $Fe_3O_4$@Pd-OA (Fig. S5, Supplementary Material) is similar to that of the magnetite SPNPs. Magnetite is an iron oxide which contains $Fe^{2+}/Fe^{3+}$ ions; when the particle size is smaller than 100 nm, magnetite can be oxidized by air to maghemite ($\gamma$-$Fe_2O_3$) through a topotactic reaction where the crystal structure is retained throughout.[43] This is very important in small NPs because the surface atoms occupy a significant space of the whole particle, and the diffusion pathway for oxygen is very short. Magnetite and maghemite can be distinguished by FT-IR spectroscopy, because magnetite presents one band at 580 $cm^{-1}$, while maghemite presents two bands at ~560 and 630 $cm^{-1}$.[44] In order to demonstrate the presence of a core–shell structure which protects the $Fe_3O_4$ core from oxidation to $\gamma$-$Fe_2O_3$ (maghemite), FT-IR spectra of $Fe_3O_4$-OA and $Fe_3O_4$@Pd-OA at different times were measured to follow this oxidation process.

In Fig. 3 the evolution with time of the IR spectra for $Fe_3O_4$-OA SPNPs and core–shell SPNPs are shown. For the bare $Fe_3O_4$-OA SPNPs the spectra show one band at 586 $cm^{-1}$ after

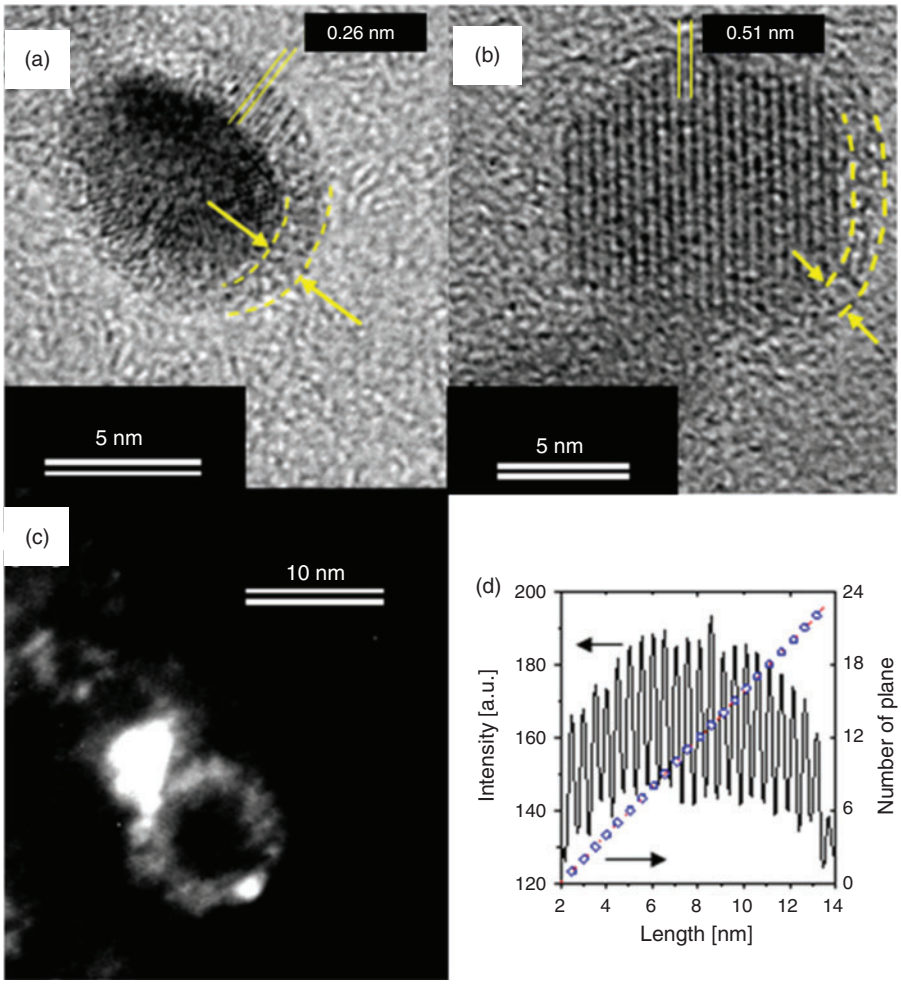


**Fig. 4.** $Fe_3O_4$@Pd-OA superparamagnetic nanoparticles. (a) High-resolution transmission electron microscopy (HRTEM) image showing the interplanar separation in the nanoparticle shell. (b) HRTEM image showing interplanar separation in the nanoparticle core. (c) Dark field image evidencing the shell on a nanoparticle. (d) Left axis, interplanar cross-section intensity of (b) core and on the right axis is the number of planes crossed as a function of the length (circles). The slope is the interplanar separation: 0.51 nm. (OA, oleylamine.)

1 day, but after 4 days two bands can be observed at 586 and 630 $cm^{-1}$, increasing the definition of these two bands with time (Fig. 3a). In the case of the core–shell SPNPs (Fig. 3b), this effect is much less pronounced and it can be clearly seen that it begins only after 28 days.

These results indicate that the palladium layer protects the core of magnetite for times longer than one month from oxidation to maghemite. This implies a formation of a well defined core–shell structure based on a core of $Fe_3O_4$ with a shell of $Pd^0$, stabilized with OA.

In order to confirm this well-defined core–shell formation, high resolution transmission electron microscopy (HRTEM) (Fig. S6, Supplementary Material) and Dark Field micrographs of $Fe_3O_4$@Pd-OA (Fig. 4) were performed.

The thickness of the palladium shell can be measured from the HRTEM images, giving 1.25–1.35 nm (see distance between arrows in Fig. 4a, b). The palladium shell can also be evidenced by the Dark Field images (Fig. 4c), where a 'donut' shape is detected. In Fig. 4a is distinguishable the interplanar distance of 0.26 nm. This value is close to the separation expected for the (111) plane of Pd. In addition, the core SPNPs have a highly crystalline structure, where planes separated by 0.51 nm (Fig. 4b, d) are clearly distinguished. An intensity profile, taken in a direction perpendicular to these planes, shows the oscillatory behaviour depicted in the continuous curve in Fig. 4d. Plotting the number of maximums crossed as a function of the transversal distance, we observe a linear relationship, whose slope is the interatomic distance observed in the core of the particle (0.51 nm). This distance is very close to the (111) interplanar distance in the spinel $Fe_3O_4$.

From TEM images of both systems, we performed histograms of the particle size frequency ($f(D_{TEM})$) as a function of the particle diameter ($D_{TEM}$), see Fig. 5. We measured the diameters of 565 particles for $Fe_3O_4$-OA and 351 for $Fe_3O_4$@Pd-OA to perform the histogram of sizes. The distribution of particle size can be described with a log-normal size distribution function:

$$f(x) = \frac{1}{\sqrt{2\pi}x\sigma}\exp\left\{-\frac{[\ln(x/x_0)]^2}{2\sigma^2}\right\} \quad (1)$$

where $x_0$ is the most probable value and $\sigma$ is the width of the distribution. The average value is $\langle x\rangle = x_0 e^{\sigma^2/2}$. Applying the lognormal distribution function (Eqn 1) to describe the histograms of the size of particles, we obtain the average particle size

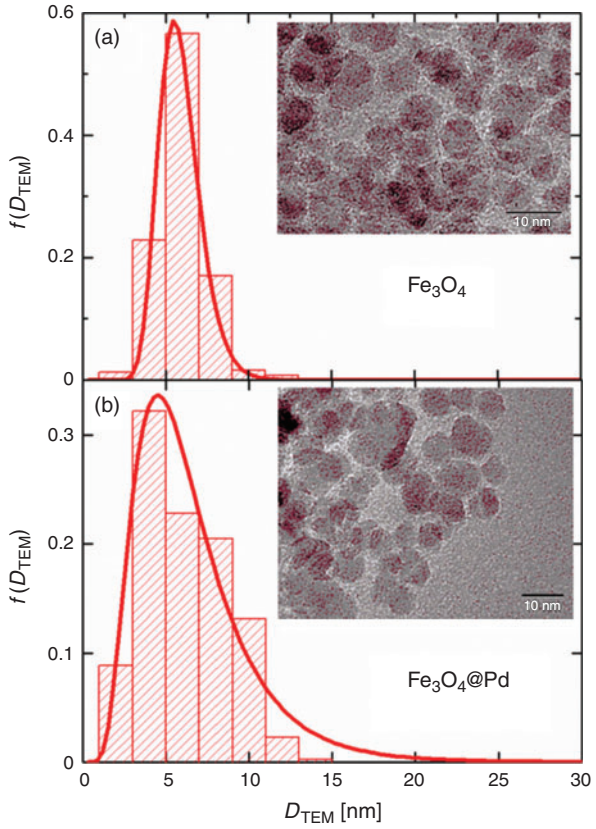


**Fig. 5.** Particle size distribution obtained from transmission electron microscopy analysis. (a) $Fe_3O_4$-OA and (b) $Fe_3O_4$@Pd-OA superparamagnetic nanoparticles (OA, oleylamine). The solid line is the log-normal distribution.

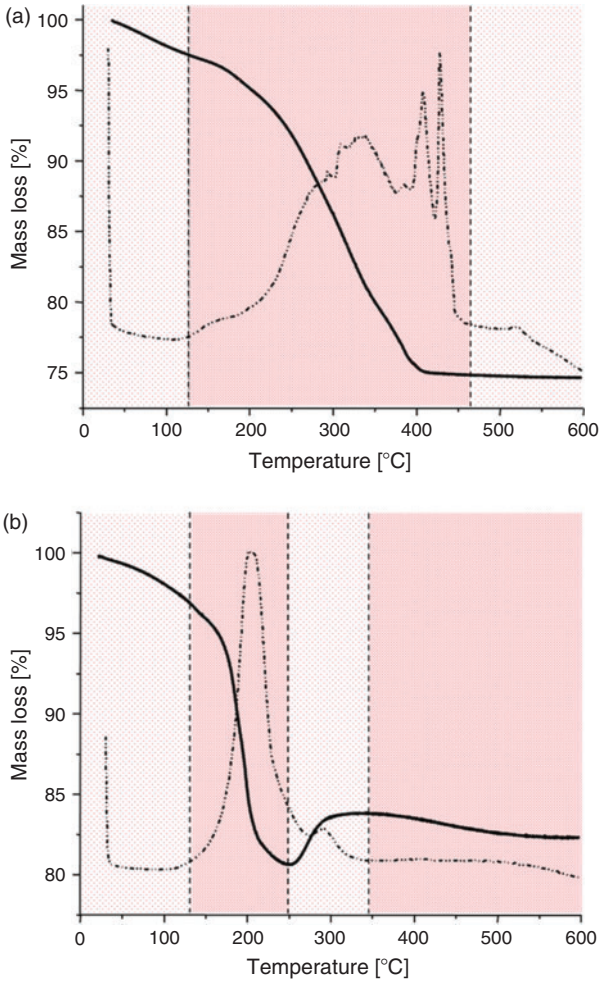


**Fig. 6.** Thermogravimetric analysis (line) and differential scanning calorimetry (dashed) curves of (a) $Fe_3O_4$-OA and (b) $Fe_3O_4$@Pd-OA superparamagnetic nanoparticles (OA, oleylamine).

and width distribution ($D_{TEM} = x$ and $\sigma_{TEM} = \sigma$) for $Fe_3O_4$-OA SPNPs: $<D_{TEM}> = 5.6 \pm 0.1$ nm, $\sigma_{TEM} = 0.23 \pm 0.02$; and for $Fe_3O_4$@Pd-OA SPNPs: $<D_{TEM}> = 5.1 \pm 0.1$ nm, $\sigma_{TEM} = 0.50 \pm 0.02$. The distribution of the $Fe_3O_4$@Pd-OA SPNPs presents a higher $\sigma_{TEM}$ than the uncovered magnetite particles. Although $<D_{TEM}>$ are similar in both systems, since $\sigma_{TEM}$ is higher for $Fe_3O_4$@Pd-OA SPNPs, these presented higher average TEM values ($<x>$) than the uncovered magnetite particles. This is another indication that the Pd is covering the magnetite cores and consequently the total size of the particles increase due to the palladium shell.

The particle size is very important for application in nanocatalysis, because the particle must have a high surface area of the catalyst (Pd) and strong magnetism, to be able to recover and reuse the catalyst. For this reason, it is desirable to minimize the amount of Pd as much as possible maintaining its catalytic activity. On the other hand, the core of magnetite needs to be greater than 2 nm, because smaller cores do not have a strong enough magnetism for magnetic recycling process.

In order to quantify the iron content (hence the magnetite content) we performed a colourimetric UV-vis experiment based on the formation of the reddish [Fe-EDTA] complex. The calibration curve and spectroscopic curves can be seen in Figs S7 and S8 (Supplementary Material). As determined by UV-vis spectroscopy, there is 0.6086 mg of $Fe_3O_4$ per mg of $Fe_3O_4$@Pd-OA (60.9 %). Fig. 6a shows the thermogravimetric (TGA) and differential scanning calorimetric (DSC) curves of $Fe_3O_4$-OA, and Fig. 6b of $Fe_3O_4$@Pd-OA. In Fig. 6a the weight loss can be attributed to loss of physically bonded water (range: room temperature–127°C, 97.5 % residue), and the decomposition of OA (range 127–460°C, 74.9 % residue). From this, it was determined that 1 mg of $Fe_3O_4$-OA SPNPs contains 0.226 mg of OA (22.6 %). In Fig. 6b the weight loss can be attributed to loss of physically bonded water (range: room temperature–127°C, 97.3 % residue), the decomposition of OA (range 127–250°C, 80.8 % residue), and the oxidation of $Pd^0$ to $Pd^{2+}$ (range: 250–345°C, 84.0 % residue). It is assumed that the entire mass gain is due to the incorporation of oxygen for formation of the species corresponding to PdO (palladium oxide). From this, it was determined that 1 mg of $Fe_3O_4$@Pd-OA SPNPs contains 0.165 mg of OA (16.5 %) and 0.206 mg of Pd (20.6 %). Considering the difference between the content of Pd and OA, we found a magnetite content of 60.2 %, which is highly consistent with the percentage of magnetite determined by UV-vis spectroscopy with a deviation of less than 1 %.

In addition, the magnetic properties were studied with magnetization ($M$) versus magnetic field ($H$), and $M$ versus $T$, using a superconducting quantum interference device (SQUID).

The magnetization as a function of temperature at $H = 50$ Oe was measured. In both samples a shift between the magnetization curves below $T_{irr} = 130$ K was observed. For $Fe_3O_4$@Pd-OA a maximum in the ZFC curve at 75 K (see Fig. 7) was

detected, while in the $Fe_3O_4$-OA it is at 70 K (not shown). The difference between the FC and ZFC magnetization curves is often used to provide information about the blocking temperature distribution, which is related to the particle volume distribution according to:

$$-\frac{d(M_{FC}(H,T)-M_{ZFC}(H,T))}{dT}\approx Tf(T_B) \quad (2)$$

where the blocking temperature distribution ($f(T_B)$) is a lognormal distribution (see Eqn 1) with $T_{B0}=x$ (the most probable blocking temperature) and $\sigma_B=\sigma$ (distribution width of the blocking temperature) being adjustable parameters. In this case we obtain $T_{B0}=8.5\pm0.5$ K and $\sigma_B=0.83\pm0.03$ and $T_{B0}=5.0\pm0.5$ K and $\sigma_B=0.98\pm0.03$ for $Fe_3O_4$-OA and $Fe_3O_4$@Pd-OA respectively. The experimental data expressed as Eqn 1, and the corresponding fit of the data with Eqn 2 are shown in Fig. 7 (only for $Fe_3O_4$@Pd-OA). An average particle diameter from the blocking temperature $<D_{TB}>$ can be obtained using the next expression:

$$\langle V\rangle = 28k_B\langle T_B\rangle/K_a=\frac{\pi}{6}\langle D_{TB}\rangle^3 \quad (3)$$

and considering

$$\langle T_B\rangle = T_{B0}e^{\sigma_B^2/2} \quad (4)$$

and $K_a\approx 5\times10^5$ erg cm$^{-3}$.[45,46] The obtained values are $<D_{TB}>\approx 6$ nm ($Fe_3O_4$) and 5 nm ($Fe_3O_4$@Pd), which are in good agreement with the TEM results. The similar TEM and magnetic volumes show that the particles are a single magnetic domain. It is important to note that in the case of $Fe_3O_4$@Pd the diameter represents the one of the magnetic core ($Fe_3O_4$).

Fig. 8 shows that $M$ versus $H/T$ taken at different temperatures presents a universal curve, which is associated with the superparamagnetic behaviour of the single magnetic domain particles. These curves can be described with a Langevin's equation:

$$M = M_s[\coth(a)-(1/a)] \quad (5)$$

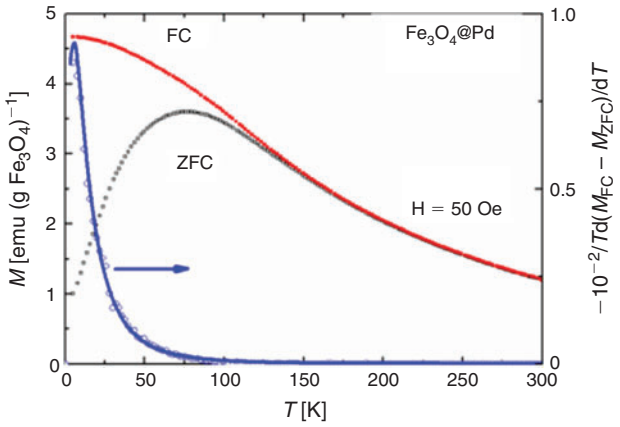


**Fig. 7.** Zero field (ZFC) and field cooled (FC) (red on line) magnetization curves versus temperature (left axis) taken at 50 Oe for $Fe_3O_4$@Pd-OA superparamagnetic nanoparticles. The right axis is plotted as a function of temperature, which is proportional to the distribution of blocking temperatures (blue circles, on line). Solid line is the fit of the experimental data with a lognormal distribution function.

where $M_s=196$ emu cm$^{-3}$ is the magnetic saturation of the NPs and $a=\mu H/k_BT$. From the $a$ parameter, the calculated average effective magnetic moment per NP is ≈3300 μB. Similar values were reported for bare $Fe_3O_4$ NPs and for NPs covered with OA.[45,46] The bulk saturation magnetization of the $Fe_3O_4$ is approximately $M_s^{bulk}\approx 470$ emu cm$^{-3}$. To obtain an estimation about the importance of the surface effects when the particle's size is reduced in many ferro- and ferrimagnetic nanocrystalline materials, the ratio between the saturation magnetization of the NPs and the bulk: $M_s/M_s^{bulk}\approx 0.42$ was calculated. Mainly the saturation magnetization is strongly affected by surface defects, such as broken bonds, vacancies, and crystalline disorder.[47] The surface layer practically does not contribute to the saturation magnetization and it is known as a 'magnetic dead layer'. In these $Fe_3O_4$@Pd-OA NPs, the width of the magnetic dead layer between 1 and 2 nm was estimated.

Fig. 9 shows the ageing effect on the NPs of $Fe_3O_4$@Pd-OA quantified through decay in the saturation magnetization at 5 K due the surface oxidation of magnetite to maghemite. Note that

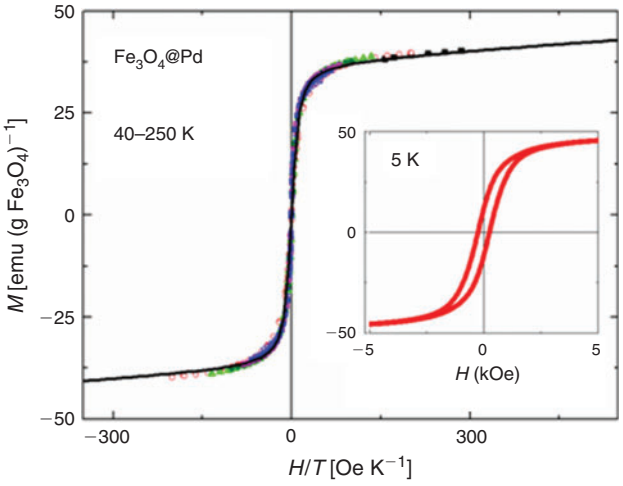


**Fig. 8.** Magnetization as a function of $H/T$ for different temperatures above the blocking temperature for $Fe_3O_4$@Pd-OA superparamagnetic nanoparticles (OA, oleylamine). Solid line is the fit with a Langevin function, which describe the superparamagnetic behaviour. In the inset, hysteresis loop showing the blocking state at 5 K.

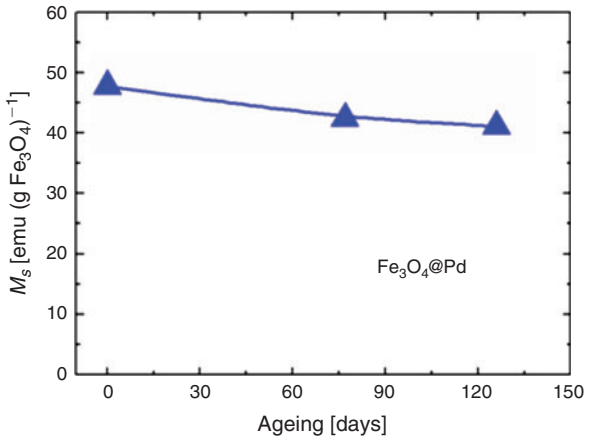


**Fig. 9.** Ageing of the $Fe_3O_4$@Pd-OA superparamagnetic nanoparticles quantified with the saturation magnetization (OA, oleylamine).

several months are needed in order to reduce 10 % of the saturation magnetization value.

### *Catalytic Performance of Pd SPNPs in the Suzuki–Miyaura Coupling Reaction*

Due to the particular usefulness of the Suzuki–Miyaura coupling reaction as a method for the formation of C–C bonds,[17–21] the catalytic activity of the newly synthesized magnetically separable $Fe_3O_4$@Pd-OA was examined in this reaction.

The catalytic efficiency of the Pd SPNPs in the coupling reaction was carried out using *p*-iodoanisole (**1**) and phenylboronic acid (**2a**). Based on our previous results,[48,49] and after a series of initial experiments, the reactions were performed with $K_3PO_4$ as the base and in the presence of 1.5 mol % of Pd, employing SPNPs $Fe_3O_4$@Pd-OA as catalyst under a nitrogen atmosphere (Fig. 10). At first, the effect of the solvent on the Suzuki–Miyaura coupling reaction with Pd SPNPs previously dispersed in different solvents was evaluated. The results are shown in Fig. 10.

With dioxane/water (50 : 50) the conversion was complete and the product *p*-methoxybiphenyl (**3a**) was obtained in 91 % yield (Fig. 10). It is important to notice that at the end of the reaction the presence of a black deposit in the wall and oil in the bottom of the Schlenk tube was observed. Under this experimental condition the catalyst was decomposed, since the surface of the Pd SPNPs could be cleaned with water, removing the stabilizer OA.[50] Moreover, the good activity of the Pd SPNPs under these conditions can be explained in terms of the water acting to wipe the surface of the catalyst leaving it more exposed for the catalysis.

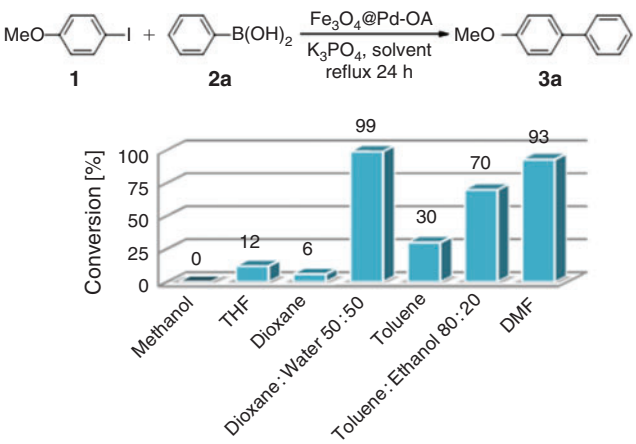


**Fig. 10.** Suzuki–Miyaura coupling reaction of *p*-iodoanisole (**1**) and phenylboronic acid (**2a**) catalyzed by $Fe_3O_4$@Pd-OA in different solvents (OA, oleylamine).

Considering these results, the use of diverse organic solvents for the reaction was explored. When the reaction of **1** with **2a** was carried out in dioxane, THF, and methanol, a low conversion of the substrate was achieved. The performance of the coupling reaction was slightly better when toluene was employed as solvent (Fig. 10). In an attempt to evaluate the base effect, the reactions in toluene with LiOAc, $Cs_2CO_3$, and $Na_2CO_3$ were performed, nevertheless product **3a** was not observed in any case. With ethanol as co-solvent in toluene (20 %) a higher conversion was observed, in addition to a lower selectivity of the reaction, unlike the other reactions the dehalogenated product anisole was obtained (24 % yields). The solvent effect is probably determined by the solubility of the base.

An improvement in the coupling reaction of **1** with boronic acid (**2a**) was observed by using DMF as solvent (Fig. 10). Further optimization studies revealed that the catalyst was inactive at room temperature, while heating the reaction mixture to 115°C gave high conversions. The coupling reaction afforded product **3a** in 80 % yield in 5 h (entry 1, Table 1). Reducing the amount of catalyst gave lower yields of the coupled product. Control experiments achieved in the absence of $Fe_3O_4$@Pd-OA confirmed that the coupling reaction did not occur in the absence of Pd (entry 2, Table 1). Also, when the reaction was carried out with only the SPNPs $Fe_3O_4$-OA the biaryl product was not obtained. Additionally, the reaction of **1** with *p*-fluorophenylboronic acid (**2b**) under the previously optimized conditions afforded a 94 % yield of the coupled product **3b** (entry 3, Table 1).

For the practical application of a catalytic system its stability and reusability are important aspects. In order to establish the recyclability of the catalyst, the Suzuki–Miyaura coupling reaction between **1** and *p*-fluorophenylboronic acid (**2b**) was selected (entry 3, Table 1). The catalyst was recovered by magnetic separation, washed with ethanol and diethyl ether respectively, dried under vacuum, and reused for the next reaction. More than 99 % of the catalyst could simply be recovered by fixing a magnet near to the reaction vessel. The $Fe_3O_4$@Pd-OA SPNPs could be recycled and reused for four

**Table 1. Suzuki–Miyaura coupling reaction of *p*-iodoanisole (1) with boronic acids catalyzed by $Fe_3O_4$@Pd-oleylamine (OA) superparamagnetic nanoparticles**

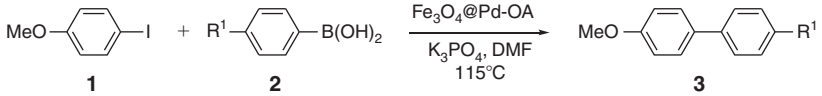


| Entry[A] | Boronic acid | [$Fe_3O_4$@Pd-OA] [mol % Pd] | Product | Time [h] | Yield[B] [%] | Conv.[C] [%] |
|---|---|---|---|---|---|---|
| 1 | **2a** | 1.5 | **3a** | 5 | 80 | 93 |
| 2 | **2a** | – | **3a** | 24 | 0 | <5 |
| 3 | **2b** | 1.5 | **3b** | 5 | 94 | 99 |

[A]Reaction conditions: 0.5 mmol of **1**, 0.75 mmol of boronic acid, 1.5 mmol of $K_3PO_4$, 4 mL of DMF, at 115°C, and under a nitrogen atmosphere.
[B]Gas chromatography yields. The yields reported represent at least the average of two reactions.
[C]Determined in relationship to the amount of initial substrate.

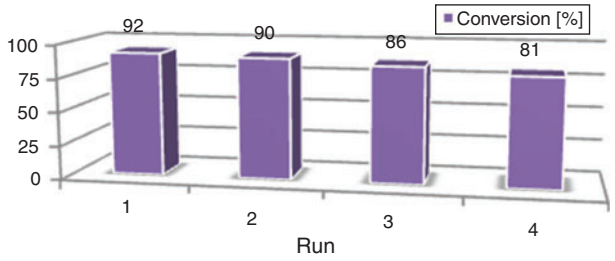


**Fig. 11.** Recyclability test for $Fe_3O_4$@Pd-OA in the Suzuki–Miyaura cross-coupling reaction of *p*-iodoanisole (**1**) and *p*-fluorophenylboronic acid (**2b**) in DMF (entry 3, Table 1) (OA, oleylamine).

consecutive times without almost any loss of their catalytic activity (Fig. 11).

## Conclusion

SPNPs of $Fe_3O_4$@Pd stabilized with OA were successfully synthesized and characterized using HRTEM, PXRD, UV-vis, DSC/TGA, FT-IR, and magnetic measurements. All results show that core–shell $Fe_3O_4$@Pd-OA SPNPs were produced with a mean diameter of the magnetic core ($Fe_3O_4$) in the order of 5 nm with a shell of Pd with an average thickness of 1.25–1.35 nm.

The synthesized $Fe_3O_4$@Pd-OA SPNPs have some notable features:

(i) simple, fast, and efficient synthesis,
(ii) high chemical stability: they can be preserved from oxidation to maghemite for several months due to the Pd shell,
(iii) a very good catalytic activity for the Suzuki–Miyaura coupling reaction,
(iv) possibility to be reused at least for four cycles, by simple magnetic separation maintaining practically the same activity.

## Experimental

### *Reagents and Instrumentation*

Urea (U, 99.99 %), $Fe(NO_3)_3{\cdot}9H_2O$ (99.999 %), $PdCl_2$ (99 %), hematite (α-$Fe_2O_3$, ≥99 %), oleylamine (OA, 70 %), dibenzyl ether (DBE, ≥98 %) and acetylacetone (Acac, ≥99 %), absolute ethanol (EtOH, ≥99.5 %), hydrochloric acid (36.5–38 %), sodium hydroxide (≥98 %), nitric acid (70 %), *n*-hexane anhydrous (95 %), diethyl ether (≥99.0 %), *p*-iodoanisole (98 %), phenylboronic acid (≥97.0 %), *p*-fluorophenylboronic acid (≥97.0 %), $K_3PO_4$ (≥98 %), and $Na_2SO_4$ (≥99.0 %) were obtained from Sigma–Aldrich and used as received. All solvents were of analytical grade and distilled before use. Toluene, THF, and dioxane were distilled under nitrogen from Na-benzophenone. DMF was stored under molecular sieves and then distilled under reduced pressure with bubbling of nitrogen. All catalytic reactions were carried out under $N_2$ atmosphere. Silica gel (0.063–0.200 mm) was used in column chromatography.

Gas chromatographic analysis was performed on a gas chromatograph with a flame ionization detector, and equipped with the following columns: HP-1 25 m × 0.20 mm × 0.25 µm column. $^1$H NMR and $^{13}$C NMR were conducted on a High Resolution Spectrometer Bruker Advance 400, in $CDCl_3$ as solvent. Gas chromatographic/mass spectrometer analysis were carried out on a GC/MS QP 5050 spectrometer equipped with a VF-5 ms, 30 m × 0.25 mm × 0.25 µm column. The characterization by PXRD was performed using a PANalytical X'Pert Pro diffractometer (40 kV, 40 mA), in Bragg–Brentano reflection geometry with $Cu_{K\alpha}$ radiation ($\lambda = 1.5418$ Å). The data were obtained between 20° and 70° 2$\theta$ in steps of 0.02 and a counting time of 24 s.

The refinement of the crystal structure was performed by the Rietveld method using the *FULLPROF* program.[51,52] A pseudo-Voigt shape function was always adequate to obtain good fits for experimental data. The magnetic measurements were performed in a commercial superconducting quantum interference device magnetometer (SQUID) on powdered samples, in the 5–300 K temperature range, and magnetic fields up to 5 T. Due to the fast oxidation of the magnetite to maghemite, the samples were sealed in quartz capsules with $N_2$ atmosphere. These were opened previous to the magnetization experiments. TEM and HRTEM images were made using a Philips CM200 (200 kV) transmission electron microscope. The samples were prepared by dropping a dispersion of NPs diluted in cyclohexane onto an ultrathin carbon-coated copper grid.

Infrared spectroscopy (FT-IR) was carried out on a Nicolet-5SXC, using KBr pellets. UV-Visible turbidimetry experiments were measured on a diode-array Shimadzu Multispec 1501 spectrophotometer, using a 1 cm path length cuvette.

TGA and DSC studies were performed on a 2950TGAHR thermogravimetric analyzer (TA Instruments) between room temperature and 600°C, and at a heating rate of 10°C min$^{-1}$, under a nitrogen flow.

### *Synthesis of Fe-Urea Complex ($[Fe(CON_2H_4)_6](NO_3)_3$)*

In a typical reaction $Fe(NO_3)_3{\cdot}9H_2O$ (5.8906 g, 19 mmol) and urea (7.0865 g, 118 mmol) were mixed (notice that a little excess of urea has been used to ensure the maximum possible yield) in 7 mL of absolute ethanol at room temperature. Concentrated $HNO_3$ (2 mL) was then added dropwise under magnetic stirring until total conversion of the yellowish solution into a light green powder. After this, the solution was centrifuged and the powder was separated and washed, first, four times with cold dry ethanol and lastly with diethyl ether. The product was dried in an oven at 45°C for 12 h. The formation of the iron-urea complex was confirmed by FT-IR spectroscopy.

### *Synthesis of $Pd(Acac)_2$*

$PdCl_2{\cdot}2H_2O$ (4.8380 g, 22.7 mmol) was transferred to a single-necked round-bottom flask and dissolved with 10–15 mL of concentrated HCl preheated to 90°C. The solution was magnetically stirred for 15 min and allowed to cool to room temperature. The cooled solution was diluted seven times with Milli-Q purified water and stirred for 10 more minutes. After this, a 4 M aqueous solution of NaOH was added dropwise to adjust the pH to 7.5–8 and to promote the precipitation of the palladium(II) acetylacetonate. The solution was centrifuged and the yellow powder obtained was separated and washed with Milli-Q water five times and dried at 55°C under vacuum. The synthesized powder was characterized by FT-IR and NMR techniques.

### *Synthesis of $Fe_3O_4$ SPNPs*

The magnetite SPNPs were prepared following a methodology previously reported,[53] using the Fe-Urea complex instead of $Fe(Acac)_3$ as a metal source and with minor changes of the reactant/solvent proportions and reactions times. In a typical reaction Fe-Urea (2.5037 g, 4.16 mmol) was dispersed in 20 mL

of OA and 20 mL of DBE at room temperature under a $N_2$ atmosphere. The dispersion was dehydrated by heating at 120°C for 40 min under magnetic stirring and then transferred to a dry three-necked round-bottom flask equipped with a reflux system, magnetic stirring, and $N_2$ atmosphere. The dispersion was heated at 10°C $min^{-1}$ up to 155°C for 1 h; later the temperature was raised at 10°C $min^{-1}$ to 300°C and kept for 60 min. The system was allowed to cool to room temperature and then aliquots of the resultant dispersion were transferred to a conical tube and diluted three times with absolute dry ethanol and centrifuged at 6000 rpm for 15 min. The as-synthesized SPNPs were washed with absolute ethanol (seven times) until no contaminants (OA, DBE, or reaction residues) were detected by FT-IR spectroscopy in the supernatant. After this, the powder was dried under vacuum at 45°C for 12 h. The SPNPs obtained were characterized by PXRD, FT-IR, TEM, and magnetization measurements.

### *Synthesis of $Fe_3O_4$@Pd SPNPs*

The core–shell SPNPs were prepared following a similar methodology to that described above for the preparation of magnetite SPNPs. The magnetite SPNPs were used as seeds for the growth of the shell of $Pd^0$. First, $Fe_3O_4$-OA (0.3828 g, 1.28 mmol of $Fe_3O_4$) and $Pd(Acac)_2$ (1.5222 g, 4.96 mmol) were dispersed in 30 mL of OA and 30 mL of DBE. The dispersion was then magnetically stirred, heated to 200°C (10°C $min^{-1}$) and kept at this temperature for 1 h in order to allow the complete decomposition of the $Pd(Acac)_2$. Finally, the dispersion was allowed to cool to room temperature, and the as-synthesized core–shell SPNPs were purified and dried following the same methodology previously described. The SPNPs obtained were characterized by PXRD, FT-IR, TEM, and magnetization measurements.

### *UV-Vis Quantification of the Content of Iron(III) in $Fe_3O_4$@Pd-OA SPNPs*

To determine the content of iron(III) in the $Fe_3O_4$@Pd-OA SPNPs, a colourimetric technique involving the formation and UV-vis quantification of the $[Fe\text{-}EDTA]^-$ complex was used. The standard procedure for preparing the solutions is detailed in the Supplementary Material. The SPNP (30 mg) samples were prepared in quintuplicate using the same standard procedure mentioned above, the exception being that a sulfonitric mixture was used instead of HCl in a final volume of 25 mL.

### *Preparation of the $Fe_3O_4$@Pd-OA SPNPs Dispersion in Organic Medium*

The dispersion of the Pd SPNPs was prepared in a Schlenk tube under nitrogen atmosphere, placing 0.0170 g of the $Fe_3O_4$@Pd-OA SPNPs and adding 10 mL of the organic solvent. This mixture was sonicated for 15 min until no more solid was observed.

### *Representative Procedure for the Suzuki–Miyaura Coupling Reaction*

The following procedure of the reaction is representative for all Suzuki–Miyaura coupling reactions. Into a 25 mL Schlenk tube with a Teflon screw-cap septum equipped with a magnetic stirrer and a nitrogen inlet, *p*-iodoanisole (**1**) (0.15 mmol), phenylboronic acid (**2a**) (0.23 mmol), and $K_3PO_4$ (0.45 mmol) were added, and three cycles of vacuum/nitrogen were performed to change to a nitrogen atmosphere. Next, 0.8 mL of DMF and 0.4 mL of $Fe_3O_4$@Pd-OA SPNPs dispersion in DMF were added. The reaction mixture was heated for 6 h in an oil bath at 115°C. After being cooled to room temperature, the mixture was open to the air, diluted with water, extracted three times with diethyl ether (10 mL each), and dried with anhydrous $Na_2SO_4$. The crude reaction was analyzed by CG and CG-MS. The biaryl product was purified by silica-gel column chromatography.

The products were characterized by $^1H$ NMR, $^{13}C$ NMR, and GC-MS analysis. All these spectroscopic data agreed with those previously reported for the following compounds: 4-methoxybiphenyl (**3a**),[54] 4-fluoro-4′-methoxybiphenyl (**3b**).[55]

#### *4-Methoxybiphenyl (**3a**)*

$\delta_H$ ($CDCl_3$) 7.56–7.30 (7H, m), 6.99–6.97 (2H, m), 3.85 (3H, s). $\delta_C$ ($CDCl_3$) 159.16, 140.84, 133.80, 128.72, 128.16, 128.75, 126.66, 114.21, 55.36. *m*/*z* (EI) 185 (14 %), 184 (100), 170 (7), 169 (52), 152 (5), 142 (6), 141 (49), 139 (10), 115 (37), 76 (7), 63 (7).

#### *4-Fluoro-4′-methoxybiphenyl (**3b**)*

$\delta_H$ ($CDCl_3$) 7.54–7.43 (m, 4H), 7.14–7.04 (m, 2H), 6.96–6.92 (m, 2H), 3.84 (s, 3H). $\delta_C$ ($CDCl_3$) 162.4 (d, *J* 244), 159.5, 137.3 (d, *J* 3.4), 133.2, 128.6 (d, *J* 8.0), 128.9, 115.9 (d, *J* 20), 114.6, 55.8. *m*/*z* (EI) 203 (13 %), 202 (100), 187 (59), 170 (7), 160 (8), 159 (78), 157 (14), 133 (41).

### *Catalyst Recycling Experiment in the Suzuki–Miyaura Coupling Reaction*

In order to perform a recyclability test, the Suzuki–Miyaura coupling reaction between *p*-iodoanisole (**1**) and *p*-fluorophenylboronic acid (**2b**) catalyzed by $Fe_3O_4$@Pd-OA SPNPs in DMF was chosen. Initially, the reaction was carried out following the procedure previously described. After the reaction mixture was heated at 115°C for 6 h, the $Fe_3O_4$@Pd-OA SPNPs was magnetically separated from the reaction mixture and washed with diethyl ether (10.0 mL × 3). They were then dried with a vacuum pump, and used directly for the next run by addition of fresh amounts of reactants. The experiment was performed four times by consecutive addition of a new batch of *p*-iodoanisole (**1**) (0.15 mmol), *p*-fluorophenylboronic acid (**2b**) (0.23 mmol), $K_3PO_4$ (0.15 mmol), and DMF (1.2 mL). The reaction mixture was then heated at 115°C for another 6 h. After this time, the reaction was monitored by CG analyses, and the amount of substrate and product was quantitatively determinate after each catalytic cycle.

## Supplementary Material

X-Ray patterns, Rietveld refinements, FT-IR spectra of $Fe_3O_4$-OA and $Fe_3O_4$@Pd-OA SPNPs, a selected area electron diffraction (SAED) pattern and a TEM image of $Fe_3O_4$-OA SPNPs, and spectral and calibration curves of $[Fe(EDTA)]^-$ are available on the Journal's website.

## Acknowledgements

The authors gratefully acknowledge financial support from CONICET, ANPCyT, and SECYT-UNC. A.L.C wishes to thank CONICET for the fellowship provided and Catalina Biglione for helpful discussion.

## References

[1] L. Vékás, *Adv. Sci. Technol.* **2008**, *54*, 127. doi:10.4028/WWW.SCIENTIFIC.NET/AST.54.127

[2] S. A. Gómez-Lopera, J. L. Arias, V. Gallardo, A. V. Delgado, *Langmuir* **2006**, *22*, 2816. doi:10.1021/LA0530079

[3] G. Frija, O. Clément, E. de Kerviler, *Invest. Radiol.* **1994**, *29*, S75. doi:10.1097/00004424-199406001-00025

[4] S. K. Jones, J. G. Winter, B. N. Gray, *Int. J. Hyperthermia* **2002**, *18*, 117. doi:10.1080/02656730110103519

[5] F. J. Lázaro, A. R. Abadía, M. S. Romero, L. Gutiérrez, J. Lázaro, M. P. Morales, *Biochim. Biophys. Acta, Mol. Basis Dis.* **2005**, *1740*, 434. doi:10.1016/J.BBADIS.2004.11.020

[6] M. Mahmoudi, H. Hofmann, B. Rothen-Rutishauser, A. Petri-Fink, *Chem. Rev.* **2012**, *112*, 2323. doi:10.1021/CR2002596

[7] A. Durdureanu-Angheluta, A. Dascalu, A. Fifere, A. Coroaba, L. Pricop, H. Chiriac, V. Tura, *J. Magn. Magn. Mater.* **2012**, *324*, 1679. doi:10.1016/J.JMMM.2011.11.062

[8] L. H. Reddy, J. L. Arias, J. Nicolas, P. Couvreur, *Chem. Rev.* **2012**, *112*, 5818. doi:10.1021/CR300068P

[9] M. Mahmoudi, A. S. Milani, P. Stroeve, *Int. J. Biomed. Nanosci. Nanotechnol.* **2010**, *1*, 164. doi:10.1504/IJBNN.2010.034651

[10] J. Salado, M. Insausti, L. Lezama, I. Gil De Muro, E. Goikolea, *Chem. Mater.* **2011**, *23*, 2879. doi:10.1021/CM200253K

[11] R. Massart, *IEEE Trans. Magn.* **1981**, *17*, 1247. doi:10.1109/TMAG.1981.1061188

[12] A. Durdureanu-Angheluta, L. Pricop, I. Stoica, C. A. Peptu, A. Dascalu, N. Marangoci, F. Doroftei, H. Chiriac, M. Pinteala, B. C. Simionescu, *J. Magn. Magn. Mater.* **2010**, *322*, 2956. doi:10.1016/J.JMMM.2010.05.013

[13] K. Woo, H. J. Lee, J.-P. Ahn, Y. Park, *Adv. Mater.* **2003**, *15*, 1761. doi:10.1002/ADMA.200305561

[14] Á. Molnár, A. Papp, K. Miklós, P. Forgo, *Chem. Commun.* **2003**, 2626. doi:10.1039/B309307G

[15] I. Favier, D. Madec, E. Teuma, M. Gomez, *Curr. Org. Chem.* **2011**, *15*, 3127. doi:10.2174/138527211797247950

[16] D. Astruc, *Inorg. Chem.* **2007**, *46*, 1884. doi:10.1021/IC062183H

[17] C. A. Fleckenstein, H. Plenio, *Chem. Soc. Rev.* **2010**, *39*, 694. doi:10.1039/B903646F

[18] N. T. S. Phan, M. Van Der Sluys, C. W. Jones, *Adv. Synth. Catal.* **2006**, *348*, 609. doi:10.1002/ADSC.200505473

[19] F. Bellina, A. Carpita, R. Rossi, *Synthesis* **2004**, *15*, 2419.

[20] S. Kotha, K. Lahiri, D. Kashinath, *Tetrahedron* **2002**, *58*, 9633. doi:10.1016/S0040-4020(02)01188-2

[21] N. Miyaura, A. Suzuki, *Chem. Rev.* **1995**, *95*, 2457. doi:10.1021/CR00039A007

[22] R. Martin, S. L. Buchwald, *Acc. Chem. Res.* **2008**, *41*, 1461. doi:10.1021/AR800036S

[23] G. C. Fu, *Acc. Chem. Res.* **2008**, *41*, 1555. doi:10.1021/AR800148F

[24] M. R. Biscoe, B. P. Fors, S. L. Buchwald, *J. Am. Chem. Soc.* **2008**, *130*, 6686. doi:10.1021/JA801137K

[25] D. M. Knapp, E. P. Gillis, M. D. Burke, *J. Am. Chem. Soc.* **2009**, *131*, 6961. doi:10.1021/JA901416P

[26] G. A. Molander, B. Canturk, *Angew. Chem. Int. Ed.* **2009**, *48*, 9240. doi:10.1002/ANIE.200904306

[27] W. Tang, A. G. Capacci, X. Wei, W. Li, A. White, N. D. Patel, J. Savoie, J. J. Gao, S. Rodriguez, B. Qu, N. Haddad, B. Z. Lu, D. Krishnamurthy, N. K. Yee, C. H. Senanayake, *Angew. Chem. Int. Ed.* **2010**, *49*, 5879. doi:10.1002/ANIE.201002404

[28] T. Kinzel, Y. Zhang, S. L. Buchwald, *J. Am. Chem. Soc.* **2010**, *132*, 14073. doi:10.1021/JA1073799

[29] V. Polshettiwar, R. Luque, A. Fihri, H. Zhu, M. Bouhrara, J.-M. Basset, *Chem. Rev.* **2011**, *111*, 3036. doi:10.1021/CR100230Z

[30] P. Li, L. Wang, L. Zhang, G. W. Wang, *Adv. Synth. Catal.* **2012**, *354*, 1307. doi:10.1002/ADSC.201100725

[31] K. K. Senapati, S. Roy, C. Borgohain, P. Phukan, *J. Mol. Catal. Chem.* **2012**, *352*, 128. doi:10.1016/J.MOLCATA.2011.10.022

[32] Q. Du, W. Zhang, H. Ma, J. Zheng, B. Zhou, Y. Li, *Tetrahedron* **2012**, *68*, 3577. doi:10.1016/J.TET.2012.03.008

[33] Z. Gao, Y. Feng, F. Cui, Z. Hua, J. Zhou, Y. Zhu, J. Shi, *J. Mol. Catal. Chem.* **2011**, *336*, 51. doi:10.1016/J.MOLCATA.2010.12.009

[34] M.-J. Jin, D.-H. Lee, *Angew. Chem. Int. Ed.* **2010**, *49*, 1119. doi:10.1002/ANIE.200905626

[35] S. Shylesh, L. Wang, W. R. Thiel, *Adv. Synth. Catal.* **2010**, *352*, 425. doi:10.1002/ADSC.200900698

[36] Y. Liao, L. He, J. Huang, J. Zhang, L. Zhuang, H. Shen, C.-Y. Su, *ACS Appl. Mater. Interfaces* **2010**, *2*, 2333. doi:10.1021/AM100354B

[37] S. Zhao, H. Y. Wu, L. Song, O. Tegus, S. Asuha, *J. Mater. Sci.* **2009**, *44*, 926. doi:10.1007/S10853-008-3192-Y

[38] S. Asuha, S. Zhao, H. Y. Wu, L. Song, O. Tegus, *J. Alloy. Comp.* **2009**, *472*, L23. doi:10.1016/J.JALLCOM.2008.05.028

[39] S. Asuha, S. Zhao, X. H. Jin, M. M. Hai, H. P. Bao, *Appl. Surf. Sci.* **2009**, *255*, 8897. doi:10.1016/J.APSUSC.2009.06.082

[40] O. Carp, L. Patron, L. Diamandescu, A. Reller, *Thermochim. Acta* **2002**, *390*, 169. doi:10.1016/S0040-6031(02)00085-0

[41] J. Luo, L. Han, N. N. Kariuki, L. Wang, D. Mott, C.-J. Zhong, T. He, *Chem. Mater.* **2005**, *17*, 5282. doi:10.1021/CM0508219

[42] J. Xie, C. Xu, N. Kohler, Y. Hou, S. Sun, *Adv. Mater.* **2007**, *19*, 3163. doi:10.1002/ADMA.200701975

[43] H. Kang, C. S. Lee, D. Kim, Y. S. Kang, Y. I. Kim, *Bull. Korean Chem. Soc.* **1998**, *19*, 408.

[44] A. G. Roca, J. F. Marco, P. Morales, C. J. Serna, *J. Phys. Chem. C* **2007**, *111*, 18577. doi:10.1021/JP075133M

[45] G. F. Goya, T. S. Berquó, F. C. Fonseca, M. P. Morales, *J. Appl. Phys.* **2003**, *94*, 3520. doi:10.1063/1.1599959

[46] E. Lima, Jr, E. De Biasi, M. Mansilla Vasquez, M. E. Saleta, F. Effenberg, L. M. Rossi, R. Cohen, H. R. Rechenberg, R. D. Zysler, *J. Appl. Phys.* **2010**, *108*, 103919. doi:10.1063/1.3514585

[47] J. Curiale, M. Granada, H. E. Troiani, R. D. Sánchez, A. G. Leyva, P. Levy, K. Samwer, *Appl. Phys. Lett.* **2009**, *95*, 043106. doi:10.1063/1.3187538

[48] P. M. Uberman, M. N. Lanteri, S. C. Parajón Puenzo, S. E. Martín, *Dalton Trans.* **2011**, *40*, 9229. doi:10.1039/C1DT10207A

[49] P. M. Uberman, L. A. Pérez, G. I. Lacconi, S. E. Martín, *J. Mol. Catal. Chem.* **2012**, *363–364*, 245. doi:10.1016/J.MOLCATA.2012.06.016

[50] V. Mazumder, S. Sun, *J. Am. Chem. Soc.* **2009**, *131*, 4588. doi:10.1021/JA9004915

[51] H. M. Rietveld, *J. Appl. Cryst.* **1969**, *2*, 65. doi:10.1107/S0021889869006558

[52] J. Rodríguez-Carvajal, *Physica B* **1993**, *192*, 55. doi:10.1016/0921-4526(93)90108-I

[53] Z. Xu, C. Shen, Y. Hou, H. Gao, S. Sun, *Chem. Mater.* **2009**, *21*, 1778. doi:10.1021/CM802978Z

[54] F.-Y. Tsai, B.-N. Lin, M.-J. Chen, C.-Y. Mou, S.-T. Liu, *Tetrahedron* **2007**, *63*, 4304. doi:10.1016/J.TET.2007.03.046

[55] A. K. Sahoo, T. Oda, Y. Nakao, T. Hiyama, *Adv. Synth. Catal.* **2004**, *346*, 1715. doi:10.1002/ADSC.200404188